Greater Kerguelen large igneous province reveals no role for mantle plume in the continental breakup of eastern Gondwana

Hugo K.H. Olierook[1,]*, Qiang Jiang[1,2], Fred Jourdan[1,2], Massimo Chiaradia[3]

[1]School of Earth and Planetary Sciences, Curtin University, GPO Box U1987, Perth, WA 6845, Australia

[2]Western Australian Argon Isotope Facility & John de Laeter Centre, Curtin University, GPO Box U1987, Perth, WA 6845, Australia

[3]Department of Earth Sciences, University of Geneva, Rue des Maraîchers 13, 1205 Geneva, Switzerland

*Compiled by / corresponding author: hugo.olierook@curtin.edu.au; +61 8 9266 7827

Abstract

The link between mantle plumes and continental breakup remain a topic of debate. Here, a new $^{40}Ar/^{39}Ar$ age of 135.9 ± 1.2 Ma (2σ) and previous ages from the Bunbury Basalt – lava flows that are part of the Greater Kerguelen large igneous province (LIP) – reveal that >80% of magmatism in the southern Perth Basin was concomitant with the continental breakup of eastern Gondwana at ca. 137–136 Ma. New and existing isotope geochemical data show that only lithospheric and depleted asthenospheric sources were melted to form the Bunbury Basalt and most other early, ca. 147–124 Ma magmatic products part of the Greater Kerguelen LIP. All lines of evidence strongly point towards passive continental breakup of eastern Gondwana, including the restriction of 147–124 Ma magmatism to continental rifts, the lack of excess oceanic magmatism in this period and the >1000 km distance between the Kerguelen plume underneath Greater Indian lithosphere and the breakup nexus. It is not possible to reconcile the influence of a thermochemical plume with the observed geochemical, spatial and geochronological information. Instead, we posit that eastern Gondwana breakup occurred proximal to the former suture zone associated with the ca. 550–500 Ma Kuunga Orogeny between Indo–Australia and Australo–Antarctica. Enrichment of the mantle with volatiles associated with subduction during the Kuunga Orogeny permitted partial melting when the continental crust was sufficiently attenuated in the Early Cretaceous. Therefore, repeated and protracted rifting of Greater India from Australo–Antarctic since the mid-Paleozoic eventually led to the rupture of the continental lithosphere and to mafic magmatism at ca. 137–136 Ma, approximately along the position of the former suture zone, without the influence of a mantle plume.

Keywords: large igneous province; Perth Basin; Bunbury Basalt; continental flood basalts; west Australian margin; $^{40}Ar/^{39}Ar$ geochronology

1 Introduction

The links between supercontinent breakup and plume-induced large igneous provinces (LIP) remain a topic of debate (Buiter and Torsvik, 2014; Condie et al., 2015; Pirajno and Santosh, 2015). The breakup of the most recent supercontinent Gondwana still remains hotly debated in spite of the fact that much more is known about the breakup of Gondwana than other supercontinents like Rodinia or Nuna (Ma et al., 2018; Olierook et al., 2016; Veevers, 2004). Part of this debate has been fueled by an uncertain relationship between the breakup of Greater India and Australo–Antarctica in eastern Gondwana and the Greater Kerguelen large igneous province, purported to have been derived from the Kerguelen mantle plume. In particular, the early magmatic products that are potentially synchronous with continental breakup remain poorly constrained.

Together with the Tethyan Himalaya igneous province, the Bunbury Basalt are the earliest recognized volcanic products that may have been driven by the Kerguelen mantle plume (Frey et al., 1996; Olierook et al., 2016; Zhu et al., 2009). Previous geochronological and 3D modelling work has established that the Bunbury Basalt erupted in at least four pulses in two paleovalleys (Coffin et al., 2002; Olierook et al., 2016; Olierook et al., 2015b). The western Bunbury Paleovalley hosts three of these four flows that were dated at 136.96 ± 0.43 Ma, 132.71 ± 0.43 Ma and 130.45 ± 0.82 Ma (Olierook et al., 2016). The oldest of these at ca. 137 Ma are synchronous with the breakup of Greater India and Australo–Antarctica at 137–136 Ma (Gibbons et al., 2012). The fourth lava flow event is present in the eastern Donnybrook Paleovalley and accounts for >50% of the preserved volume of the Bunbury Basalt (Olierook et al., 2015b). However, it has not yet been dated successfully. Thus, establishing a clear link between continental breakup and the Bunbury Basalt and, in turn, whether a mantle plume was implicated requires a comprehensive understanding of the entire Bunbury Basalt, not just the western portion. Isotope geochemical data paint an enigmatic picture in that most of the Greater Kerguelen large igneous province, including the main Southern and Central Kerguelen

Plateau magmatic constructs, do not show any evidence of melt from the Kerguelen plume head but only comprise depleted asthenosphere and lithospheric products (Frey et al., 1996; Ingle et al., 2004; Liu et al., 2015; Ma et al., 2018; Olierook et al., 2016; Olierook et al., 2017). This picture is also significantly fragmented in that only two isotope geochemical analyses are from the older ca. 137 Ma flows in the Bunbury Basalt (Frey et al., 1996). There is little evidence for any evolution of mantle sources for the Bunbury Basalt, which again precludes a definitive link to whether a mantle plume was necessary.

To solve the conundrum on whether the Kerguelen mantle plume played a role in the production of the Bunbury Basalt and the breakup of eastern Gondwana, we provide five new step-heated plagioclase $^{40}Ar/^{39}Ar$ ages from the eastern paleovalley of the Bunbury Basalt lava flows. Geochronological data is complemented with new Sr–Nd–Pb isotopic geochemical data from all known Bunbury Basalt lava flows to assess the evolution of mantle sources. Together, geochronological and isotope geochemical data allow a robust evaluation of the drivers for magmatism in onshore Western Australia and, ultimately, whether a magma plume was involved in triggering the breakup of eastern Gondwana.

2 Geological Setting of the Bunbury Basalt

The Bunbury Basalt comprises a series of lava flows and possible scarce sheeted intrusive rocks in the southern Perth Basin of Western Australia (see Olierook and Timms, 2016; Olierook et al., 2015c and references therein for recent tectonic and stratigraphic reviews of the Perth Basin). During the Early Cretaceous, the Bunbury Basalt lava flows erupted from vent sites postulated to lie at intersections of minor faults with the basin-bounding Darling Fault (Fig. 1b; Olierook et al., 2015b). They were extruded as four distinct lava flow events into two deeply-incised paleovalleys that form the Valanginian breakup unconformity (Olierook et al., 2015b).

The western paleovalley, the Bunbury Paleovalley, host three of the four flows and preserves some ~43 km^3 of mafic lava. Two of these flows in the Bunbury Paleovalley – a lower and upper flow – were dated at ca. 137 and 133 Ma, respectively, and comprise the bulk of the ~43 km^3 (Olierook et al., 2016; Olierook et al., 2015b). Up to 5m of interflow siltstone and claystone separate the two flows in the Bunbury Paleovalley (Backhouse, 1988). The upper flow only defines the top ~10 m of the western paleovalley (Olierook et al., 2015b). On the basis of an average thickness of ~30 m of mafic lava in the western paleovalley (Olierook et al., 2015b), the upper flow comprises ~14 km^3 and the lower flow 29 km^3 of mafic lava. The third lava flow in the Bunbury Paleovalley is situated at its southern end along the southern coast at a locality called Black Point (Olierook et al., 2015b). Black Point was originally thought to record one of the two flows within the Bunbury Paleovalley (Olierook et al., 2015b) but was subsequently dated at ca. 130.5 Ma, revealing a distinct age and geochemistry (Olierook et al., 2016).

The eastern paleovalley, the Donnybrook Paleovalley, hosts ~47 km^3 of mafic lava in a continuous layer averaging 70 m in thickness, which is interpreted to be a single flow (Olierook et al., 2015b). No interflow sediment is present.

Possibly comagmatic, deep-seated, discontinuous dolerite bodies intruded into Permian and Triassic sedimentary rocks at depths of 2700–4600 m below sea level (Olierook et al., 2015b; Poynton and Hollams, 1980; Union Oil Development Corporation, 1972; Wharton, 1981; Williams and Nicholls, 1966). The intrusive bodies have been analyzed using plagioclase $^{40}Ar/^{39}Ar$ geochronology but failed to yield a reliable age on all occasions (Olierook et al., 2016). The age spectra of the intrusive bodies are compatible with scenarios involving (1) the presence of excess $^{40}Ar^*$ affecting Early Cretaceous sills, or (2) a Precambrian crystallization age, thus unrelated to the emplacement of the Greater Kerguelen large igneous province.

The vast majority of age, isotopic and chemical data is taken from the western of the two channels, the Bunbury Paleovalley (Coffin et al., 2002; Frey et al., 1996; Olierook et al., 2016). The Bunbury Paleovalley shows an overall negative magnetic anomaly with respect to the present-day magnetic field, implying that at least the thicker lower flow erupted during a period of reversed magnetic polarity (Olierook et al., 2015b). The eastern Donnybrook Paleovalley has a positive magnetic anomaly, indicating that the magmas were emplaced during a period of normal magnetic polarity; i.e., indicating an eruption time that was temporally distinct to both lava flows in the Bunbury Paleovalley. However, there were ~35 magnetic reversals in the Valanginian and Hauterivian (139.4–130.8 Ma), with periods of normal or reversed polarity lasting as little as ~20 ka (Ogg, 2012). Our $^{40}Ar/^{39}Ar$ ages – with analytical uncertainties of >0.4 Ma – will therefore not necessarily resolve age differences for flows erupted during periods of opposing magnetic polarity. It is presently uncertain what the temporal relationship between the two paleovalleys is, and how the paleodrainage system evolved during continental breakup (Olierook et al., 2015b).

3 Sample selection

For $^{40}Ar/^{39}Ar$ geochronology, five ~20 cm-long, quarter-core, basaltic andesite samples (BN25–BN29) were collected from two drill cores that penetrate through a single ~70 m thick lava flow in the Donnybrook Paleovalley (Fig. 1b, Table 1, Supplementary Table A). These two drill cores, DDB-7 and DDB-8, together with a few weathered outcrop localities, are the only rocks available for sampling that unambiguously belong to the Donnybrook Paleovalley (Morant, 1988; Playford et al., 1976). Differentiating between the Bunbury and Donnybrook paleovalleys relies upon magnetic data and drill hole constraints that were used to build the 3D model of the Bunbury Basalt (Olierook et al., 2015b). Both DDB-7 and DDB-8 clearly belong to the Donnybrook Paleovalley, in which the lava flow has a normal magnetic polarity. Hand specimens indicate the Bunbury Basalt in DDB-7 and

DDB-8 comprises dark grey, sparsely vesicular, porphyritic mafic rocks with fine-grained groundmass. All samples contain ~20% plagioclase phenocrysts up to 250 μm long with a groundmass of plagioclase, pyroxene and opaque minerals. The only noticeable variability in samples is the absence of pyrite towards the top, and progressively more pyrite towards the base of the flow.

For Sr–Nd–Pb isotope geochemistry, nine mafic lava samples from the Bunbury Basalt were analyzed, including four of the five newly collected samples (see Supplementary Table B). The other five samples were selected from sites where reliable $^{40}Ar/^{39}Ar$ ages were previously obtained (Olierook et al., 2016), including two samples from Donnelly River (ca. 137 Ma), one sample from each of the lower and upper flow of the Gelorup Quarry (ca. 137 Ma and 133 Ma, respectively) and one sample from Black Point (ca. 130 Ma, Fig. 1).

4 Analytical techniques

4.1 $^{40}Ar/^{39}Ar$ geochronology

All five samples from both drill cores were dated using $^{40}Ar/^{39}Ar$ geochronology. Samples were crushed and minerals were separated using a Frantz magnetic separator. The non-magnetic fraction was carefully hand-picked under a binocular microscope to select unaltered, optically transparent, 125–212 μm-size plagioclase grains. In all cases, picked plagioclase crystals were optically transparent when viewed under a binocular microscope and free from inclusions. The selected plagioclase grains were leached in diluted (5N) HF for one minute and then thoroughly rinsed with distilled water in an ultrasonic cleaner. Samples were loaded into several large wells of 1.9 cm diameter and 0.3 cm depth aluminum discs. The discs were Cd-shielded (to minimize undesirable nuclear interference reactions) and irradiated for 40 hours in the TRIGA nuclear reactor (Colorado, USA) in central position.

The $^{40}Ar/^{39}Ar$ analyses were performed on an ARGUS VI at the Western Australian Argon Isotope Facility at Curtin University. The ages were calculated relative to GA1550 biotite neutron flux monitor, for which an age of 99.738 ± 0.104 Ma was used (Renne et al., 2011). The mean J-values computed from standard grains are 0.01085900 ± 0.00000923 (0.08%), determined as the average and standard deviation of J-values of the small wells for the irradiation disc. Mass discrimination was calculated using a power law and monitored using an automated air pipette, providing a mean value of 0.992403 ± 0.000397 (0.04%) per dalton. The correction factors for interfering isotopes were $(^{39}Ar/^{37}Ar)_{Ca} = 6.95 \times 10^{-4}$ (± 1.3%), $(^{36}Ar/^{37}Ar)_{Ca} = 2.65 \times 10^{-4}$ (± 0.8%) and $(^{40}Ar/^{39}Ar)_{K} = 7.30 \times 10^{-4}$ (± 12%). Modern atmospheric argon was considered to be 298.56 ± 0.31 (Lee et al., 2006). Additional constants, ratios and all $^{40}Ar/^{39}Ar$ data may be found in Supplementary Table A.

Our criteria for the determination of plateaus are as follows: (i) plateaus must include at least 70% of ^{39}Ar, and (ii) the plateaus should be distributed over a minimum of three consecutive steps agreeing at 95% confidence level and satisfying a probability of fit (p) of at least 0.05. Plateau ages are given at the 2σ level and are calculated using the mean of all the plateau steps, each weighted by the inverse variance of their individual analytical error. All sources of uncertainties are included in the calculation, including the decay constants.

4.2 Sr–Nd–Pb isotope geochemistry

Radiogenic isotope ratios of Sr ($^{87}Sr/^{86}Sr$), Nd ($^{143}Nd/^{144}Nd$) and Pb ($^{206}Pb/^{204}Pb$, $^{207}Pb/^{204}Pb$, $^{208}Pb/^{204}Pb$) were measured at the University of Geneva, Switzerland. The method is described in detail in Béguelin et al. (2015). Between 100 and 120 mg of whole rock powder were dissolved for 7 days in Savillex® Teflon vials using 4 ml of concentrated HF and 1 ml of HNO_3 14M, at a temperature of 140 °C and with the help of ultrasonication for 30 minutes twice a day. Subsequently, samples were dried and re-dissolved for 3 days (also with 30 minutes ultrasonication twice a day) in 3 ml of HNO_3 14M and dried again. Sr, Nd and Pb were then separated using cascade columns with Sr-Spec, TRU-Spec and Ln-Spec resins according to a protocol modified from Pin et al. (1994). Finally, the material was redissolved in 2% HNO_3 solutions and ratios were measured using a Thermo Neptune PLUS Multi-Collector ICP-MS in static mode. Ratios used to monitor internal fractionation were: $^{88}Sr/^{86}Sr$ = 8.375209 for the $^{87}Sr/^{86}Sr$ ratio, $^{146}Nd/^{144}Nd$ = 0.7219 for the $^{143}Nd/^{144}Nd$ ratio and $^{203}Tl/^{205}Tl$ = 0.418922 for the three Pb ratios (a Tl standard was added to the solution). External standards used were SRM987 ($^{87}Sr/^{86}Sr$ = 0.710248, long-term external reproducibility: 10 ppm, 1σ; McArthur et al., 2001), JNdi-1 ($^{143}Nd/^{144}Nd$ = 0.512115; long-term external reproducibility: 10 ppm, 1σ; Tanaka et al., 2000), and SRM981 for Pb (long-term 1σ external reproducibility of 0.0082% for $^{206}Pb/^{204}Pb$, 0.0064% for $^{207}Pb/^{204}Pb$ and 0.0094% for $^{208}Pb/^{204}Pb$; Baker et al., 2004). $^{87}Sr/^{86}Sr$, $^{143}Nd/^{144}Nd$ and Pb isotope ratios were further corrected for external fractionation (due to a systematic difference between measured and accepted standard ratios) by a value of –0.021‰, +0.051‰ and +0.36‰ amu respectively. Interferences at masses 84 (^{84}Kr), 86 (^{86}Kr) and 87 (^{87}Rb) were corrected by monitoring ^{83}Kr and ^{85}Rb, ^{144}Sm interference on ^{144}Nd was monitored on the mass ^{147}Sm and corrected by using a $^{144}Sm/^{147}Sm$ value of 0.206700 and ^{204}Hg interference on ^{204}Pb was corrected by monitoring ^{202}Hg. Total procedural blanks were <500 pg for Pb and <100 pg for Sr and Nd which are insignificant compared to the amounts of these elements purified from the investigated whole rock samples.

5 Results

5.1 $^{40}Ar/^{39}Ar$ age results of the Donnybrook Paleovalley, Bunbury Basalt

Five plateau ages were obtained from six analyses, with ages ranging between 138.7 ± 2.4 and 133.7 ± 2.8 (2σ, Table 2, Fig. 2). All ages are indistinguishable within error. Given that these were from the same flow, a weighted mean of the plateau steps (*n* = 92) was calculated, yielding an age of 135.9 ±

1.2 (MSWD = 0.63; p = 1.00; Fig. 3). Ratios of K/Ca (0.0017–0.0018; Ca/K = 560–590) are indicative of fresh plagioclase rather than alteration products (Fig. 2; Verati and Jourdan, 2014). Such low K/Ca values explain why the individual plateau ages have relatively low precision compared to more 'conventional' LIP plagioclase compositions despite using similar analytical conditions (e.g., 181.4 ± 0.4 Ma for plagioclase dolerites from the Ferrar LIP; Ware and Jourdan, 2018). The age of 135.9 ± 1.2 Ma (2σ) is considered the crystallization age of the eruption that extruded into the Donnybrook Paleovalley.

5.2 Sr–Nd–Pb isotope geochemical results from the Bunbury Basalt

The ca. 136 Ma Donnybrook Paleovalley (BN25, 26, 28, 29) shows Sr–Nd–Pb isotopic ratios that are very similar to Black Point (ca. 130 Ma, Figs. 1, 4) and are thus considered part of the 'Gosselin-type' geochemical group (Gosselin is an alternative name for Black Point; Frey et al., 1996). Both the upper (BN3, ca. 133 Ma) and lower (BN4, ca. 137 Ma) flows in Gelorup Quarry are similar to the 'Casuarina-type' magmas, named after Casuarina Point (Fig. 1; Frey et al., 1996). The Gosselin-type analyses have higher $^{87}Sr/^{86}Sr$ (>0.706), lower $^{143}Nd/^{144}Nd$ (<0.5125) and higher $^{207}Pb/^{204}Pb$ ratios (>15.6) compared to the Casuarina-type analyses (Fig. 4). Sample BN22 and BN10 from the Donnelly River and Black Point, respectively, are very similar in Sr–Nd–Pb composition to previously acquired samples from these sites (Frey et al., 1996). Sample BN21 shows anomalously high measured $^{87}Sr/^{86}Sr$ (~0.716), $^{206}Pb/^{204}Pb$ (~18.7) and $^{208}Pb/^{204}Pb$ (~40.1) isotopic ratios. Given BN21 is from the same unit as BN22 and that BN22 yielded comparable isotopic ratios to previous studies (Frey et al., 1996), we consider the analyses from BN21 unreliable.

6 Discussion

6.1 *Age and distribution of the Bunbury Basalt*

Prior to this study, the Bunbury Basalt had been characterized by reliable $^{40}Ar/^{39}Ar$ ages from four localities, yielding three different populations at ca. 137 Ma, 133 Ma and 130.5 Ma (Fig. 1; Coffin et al., 2002; Olierook et al., 2016). The oldest age population was obtained from the lower of the two flows of the western Bunbury Paleovalley at both its southern extremity and near its northern margin (Olierook et al., 2015b). Here, we add a robust age of 135.9 ± 1.2 Ma for the Donnybrook Paleovalley (Fig. 2). Although this new age is indistinguishable from the oldest age of 136.96 ± 0.43 Ma obtained on the lower flow in the Bunbury Paleovalley (Olierook et al., 2016), magnetic polarity differences indicate that these represent separate lava flows. Nevertheless, most Bunbury Basalt magmatism occurred at ca. 137–136 Ma and was spatially ubiquitous across the southern Perth Basin, both within the Donnybrook Paleovalley and as part of the lower flow of the Bunbury Paleovalley. A first order volume calculation using the model of Olierook et al. (2015b) shows that the preserved volume of magmatism erupted at 137–136 Ma is >80% of the total volume of the Bunbury Basalt (73 km^3). A significant temporal gap separates the ca. 137–136 Ma lava flows from the younger ca. 133 and 130.5 Ma eruptive products. The younger magmatic events were also spatially restricted. The ca. 133 Ma younger lava flows were confined to the western of the two paleovalleys, which can be traced via aeromagnetic and drillhole data from north to south. The youngest eruptions of ca. 130.5 Ma were from an isolated locality, Black Point, which probably represents the final burst of volcanism in onshore Australia.

The configuration of the paleodrainage system into which the Bunbury Basalt flowed also provides evidence of the migration of continental breakup. The paleodrainage system was initially widely laterally distributed across the southern Perth Basin at ca. 137–136 Ma (Fig. 5a). At ca. 133 Ma, magmatism was confined to the western paleovalley. By ca. 130.5 Ma, magmatism was restricted to Black Point. The implication here is that the drainage system preferentially avulsed towards the west and south. This drainage avulsion probably occurred as fault blocks tilted westwards and southwards towards the breakup nexus (Figs. 1 and 5; Olierook et al., 2019). Recent age data from the Naturaliste Plateau ranging from ca. 132 to ≥128 Ma further support the hypothesis that magmatism proceeded from east (onshore southwestern Australia) to west (offshore western Australia, Fig. 5b; Direen et al., 2017; Olierook et al., 2017). Despite the spatial and volumetric progression of magmatism from ca. 137–130 Ma, there is no systematic evolution of mantle sources with time (Fig. 4). Therefore, the proportion of melt sources is independent of the spatial and volumetric magmatic progression.

6.2 Was the Kerguelen plume required to produce the Bunbury Basalt?

The link between the Kerguelen LIP and Bunbury Basalt was originally made on near-synchronicity, similar geochemical signatures and relatively close spatial association (Frey et al., 1996). However, recent $^{40}Ar/^{39}Ar$ age data (Olierook et al., 2016; this study) have since been refined to reveal a ~10 Myr age gap between the last igneous activity associated with the Bunbury Basalt (ca. 130 Ma) and the earliest eruption dated for the Southern Kerguelen Plateau (ca. 120 Ma; Fig. 6; Duncan, 2002). Moreover, there is also a paucity of age data in other eastern Gondwanan provinces during 130–120 Ma, with the sole exception of the Wallaby Plateau (ca. 124 Ma, Fig. 6; Olierook et al., 2015a). Geochemically, it is well established that the Bunbury Basalt shares isotopic similarities with Early Cretaceous magmatism from the Kerguelen Plateau, Broken Ridge and other circum-Indian Ocean magmatic products (Fig. 7; Olierook et al., 2017). However, the involvement of any plume melt has yet to be demonstrated for most magmatic products associated with the Kerguelen LIP prior to ca. 100 Ma. The exception is the ca. 147–115 Ma Tethyan Himalaya igneous province, where a mixture of Greater Indian continental crust and Kerguelen plume melt is likely (Fig. 7; Ghatak and Basu, 2011; Liu et al., 2015; Olierook et al., 2017).

The Tethyan Himalaya igneous province holds the key for ascertaining the composition of the Kerguelen plume head given that independently constrained plate–plume reconstructions place the plume head underneath northern Greater India, directly below the Tethyan Himalaya (Doubrovine et al., 2012; Gibbons et al., 2013; Watson et al., 2016; Whittaker et al., 2013). The simplest method to explain the Sr–Nd–Pb isotopic composition for the ca. 147–115 Ma Tethyan Himalaya is a mixture between Greater Indian continental crust (Ghatak and Basu, 2011) and the Kerguelen plume, specifically the composition attributed to the Kerguelen plume tail (see discussion in Olierook et al., 2017; Weis et al., 1993). It follows that the Kerguelen plume head and plume tail have the same composition, and that significant proportions of plume melt are only present in the post-100 Ma Greater Kerguelen LIP (except the Tethyan Himalaya). Alternative methods of invoking a plume head composition between a lithospheric and asthenospheric end-member are possible (Ingle et al., 2003) but are not necessary to explain the Sr–Nd–Pb isotopic compositions for the pre-100 Ma Greater Kerguelen LIP. Moreover, these models were made prior to and fail to account for the composition of the Tethyan Himalaya igneous province. Therefore, the simplest and most plausible explanation is that all other pre-100 Ma products can be explained by a mixture of asthenospheric and lithospheric (mantle and/or crust) sources without any thermochemical plume involvement (Fig. 7; Olierook et al., 2017).

One other crucial aspect that is poorly explained by a mantle plume model is the distribution of the early (pre-120 Ma) magmatic products. If a mantle plume is invoked, the magmatic products in the Tethyan Himalaya, the eastern Indian Ocean and onshore Western Australia require a ~2000 km diameter plume head (Fig. 8). Such distances are not impossible for mantle plumes but are at odds with where magmatism occurs and, just as importantly, where magmatism is absent (Figs. 1 and 8).

All early magmatic products of the Greater Kerguelen LIP are exclusively associated with continental rifts, including the ca. 147–115 Ma Comei province (Chen et al., 2018), the 137–130 Ma Bunbury

Basalt (Olierook et al., 2016), the ca. 130 Ma Naturaliste Plateau (Direen et al., 2017; Olierook et al., 2017) and the ca. 124 Ma Wallaby Plateau (Olierook et al., 2015a). All of these regions eventually formed into continental margins or microcontinents, attesting to the importance of continental and subcontinental lithosphere in magmatic production (Olierook et al., 2017).

In contrast, the nascent eastern Indian Ocean that separated all these distinct (micro)continental provinces exhibits a bathymetry that is typical for mid-oceanic crustal production without excess magmatism caused by a mantle plume (White et al., 1992). Using the 1° × 1° crustal thickness model of Laske et al. (2013) (CRUST 1.0: https://igppweb.ucsd.edu/~gabi/crust1.html), we compute an oceanic crustal thickness of 7.1 ± 0.8 km (2σ) for the Perth Abyssal Plain (i.e., the earliest portions of oceanic crust following the breakup of eastern Gondwana), negating areas covered by any microcontinents. Such oceanic crustal thickness is compatible with standard 7 ± 1 km oceanic crustal thickness formed at medium to fast-spreading mid-ocean ridges (Laske et al., 2013; Meier et al., 2007; White et al., 1992; Young et al., 2018). The implication is that excessive magmatism in the oceanic realm did not occur during the breakup of Gondwana, such as would be caused by the interaction of a mantle plume and oceanic crust (Bown and White, 1994). Although it is likely that a mantle plume was present underneath Greater India as far back as 147 Ma (Figs. 7, 8; Shi et al., 2018), it is difficult to envisage how magmatism was produced in southwest Australia and at microcontinents in the eastern Indian Ocean without additional magmatism in the nascent ocean basin. As the oceanic crust is significantly thinner than the continental crust, any thermal anomaly underneath Greater India would not be able to produce magmatism in southwest Australia as it would first have to impinge and decompress in the nascent Indian Ocean lithosphere. Therefore, if the plume–plate models are correct in placing the Kerguelen mantle plume under Greater India until at least ca. 100 Ma (e.g., Doubrovine et al., 2012), then the 137–130 Ma Bunbury Basalt, the ca. 130 Ma Naturaliste Plateau and the ca. 124 Ma Wallaby Plateau could not have had a mantle plume implicated in their geneses.

6.3 Causes of the breakup of eastern Gondwana

If a thermochemical plume was not responsible for the magmatic products in southwestern Australia and in the eastern Indian Ocean, it follows that a mantle plume did not trigger the breakup of eastern Gondwana at 137–136 Ma. Yet, the synchronicity of the earliest magmatism in southwestern Australia and continental breakup of Greater India and Australo–Antarctica at ca. 137–136 Ma, and migration of paleodrainage systems towards the breakup nexus, implies that the cause of magmatism was also the cause of continental breakup (Fig. 8).

Rifting in the Perth Basin first occurred in the mid-Paleozoic (Hocking, 1991; Markwitz et al., 2017). Since then, repeated and protracted rifting in the Perth Basin has meant that the lithosphere between Greater India and Australo-Antarctica had already been weakened well before the breakup of these continental bodies in the Early Cretaceous (Harris, 1994; Olierook et al., 2015c; Song and Cawood, 2000). The earliest magmatic products in southwestern Australia could instead be derived solely from passive rifting, leading to decompression of the asthenosphere and subsequent emplacement of tholeiitic Bunbury Basalt. However, the present-day thickness of the continental crust in southwestern Australia is insufficiently attenuated ($\beta \approx 1.4$) to facilitate decompression melting of anhydrous, upper mantle peridotite (Chappell and Kusznir, 2008; Olierook et al., 2016). Therefore, either an additional heat source or a fertile mantle is necessary to produce the Bunbury Basalt and trigger the breakup of eastern Gondwana.

Other than mantle plumes, one plausible mechanism to elevate mantle temperatures is via mantle warming under supercontinents, which can elevate upper mantle temperatures by >100 °C (Coltice et al., 2007) and may produce large igneous provinces as extensive as the Central Atlantic magmatic province (Marzoli et al., 2018). Eastern Gondwana had formed by ca. 500 Ma during the Kuunga Orogeny (Daczko et al., 2018; Halpin et al., 2017), so enough time had elapsed to elevate mantle temperatures underneath the Gondwanan supercontinent. However, mantle warming under supercontinents only occurs distal (>1000 km) from all oceanic crust, so that the mantle is effectively insulated (Coltice et al., 2007). Greater India's and Australia's northern margins were adjacent to the Neotethys Ocean and <700 km from the site of continental breakup in the Perth Abyssal Plain (Fig. 8). Thus, mantle warming is probably not a plausible mechanism to explain the production of Bunbury Basalt and other magmatic provinces part of the Greater Kerguelen LIP.

Rather than an additional heat source, we propose that the mantle underneath eastern Gondwana was hydrated, facilitating decompression melting at significantly lower temperatures to produce the Bunbury Basalt and aid in promoting continental breakup (Olierook et al., 2016). Geochemical evidence such as Nb and Ta depletions, enrichment in large ion lithophile elements and high $^{207}Pb/^{206}Pb$ for $^{206}Pb/^{204}Pb$ isotopic ratios are all compatible with an ancient subcontinental lithospheric mantle that has been modified and made fertile through subduction processes (Murphy et al., 2002; Olierook et al., 2017). The key to the position of continental breakup is the location of the original suture of Indo–Antarctica with Australo–Antarctica along the Pinjarra Orogen during the Kuunga Orogeny (Aitken et al., 2016; Fitzsimons, 2003; Halpin et al., 2017). The inherent lithospheric structural discontinuity between these two terranes was probably the primary reason why continental breakup occurred here (Buiter and Torsvik, 2014; Mole et al., 2014; Will and Frimmel, 2018). The Pinjarra Orogen suture was a zone of lithospheric weakness that was easier to exploit than any other parts of the far thicker Greater Indian, Australian or Antarctic lithosphere. Continental breakup thereby employed approximately the same zone as where it was originally sutured together. Additionally, either collision associated with the Kuunga Orogeny (Halpin et al., 2017) or the subduction along the entire southern margin of Gondwana (Veevers, 2004) enriched the lithospheric mantle in volatiles, as evidenced by significant lithospheric geochemical components in the Greater Kerguelen LIP magmatic products (Fig. 7; Olierook et al., 2017). We advocate that this enrichment was sufficient in promoting partial melting of the mantle without necessitating an additional heat source to induce melting. Successive rifting events from the mid-Paleozoic through to the Early Cretaceous eventually attenuated the continental lithosphere sufficiently to permit partial melting of this enriched lithospheric mantle, all of which eventually led to the passive continental breakup of eastern Gondwana at ca. 137–136 Ma without a thermochemical plume.

7 Conclusions

New and previously published geochronological data from the Bunbury Basalt – lava flows that are part of the Greater Kerguelen large igneous province – reveal that >80% of magmatism in the southern Perth Basin was concomitant with the continental breakup of eastern Gondwana at ca. 137–136 Ma. Radiogenic isotope data show that only lithospheric and depleted asthenospheric sources were melted to form the Bunbury Basalt and other early circum-eastern Gondwana magmatic products part of the Greater Kerguelen LIP (with the Tethyan Himalaya as an exception). The >1000 km distance between the Kerguelen plume underneath Greater Indian lithosphere and the breakup nexus, the restriction of 147–124 Ma magmatism to continental rifts, and the lack of excess oceanic magmatism in this period all strongly point towards a passive continental breakup of eastern Gondwana. It is not possible to reconcile the influence of a thermochemical plume with the observed geochemical, spatial and geochronological information. We propose that the position of eastern Gondwana breakup is strongly linked to the former location of the suture zone associated with the ca. 550–500 Ma Kuunga Orogeny between Indo–Australia and Australo–Antarctica. Enrichment of the mantle with volatiles associated with subduction during the Kuunga Orogeny permitted partial melting when attenuation of the continental crust was sufficient in the Early Cretaceous. Ultimately, repeated and protracted rifting of Greater India from Australo–Antarctic since the mid-Paleozoic eventually led to the rupture of the continental lithosphere and mafic magmatism at ca. 137–136 Ma, approximately along the position of the former suture zone, without the influence of the Kerguelen mantle plume.

Acknowledgements

The authors would like to thank the Geological Survey of WA for their access to core and drill cuttings, and C. Mayers and R.A. Frew in the WA Argon lab for help in sample preparation and analysis. We thank the detailed comments from two anonymous reviewers and the editorial handling of T. A. Mathers. This work was funded by Australian Antarctic Science Project #4444 and #4446. QJ acknowledges support of a CSC–CIPRS scholarship.

References

Aitken, A.R.A., Betts, P.G., Young, D.A., Blankenship, D.D., Roberts, J.L., Siegert, M.J., 2016. The Australo-Antarctic Columbia to Gondwana transition. Gondwana Research 29, 136-152.

Amante, C., Eakins, B.W., 2009. ETOPO1 1 Arc-Minute Global Relief Model: Procedures, Data Sources and Analysis, NOAA Technical Memorandum NESDIS NGDC-24. National Geophysical Data Center, NOAA [24 June 2014].

Backhouse, J., 1988. Palynology of Cowaramup Line 7A: Western Australia. Geological Survey of Western Australia, Perth, <retrieved from http://geodocs.dmp.wa.gov.au/>.

Baker, J., Peate, D., Waight, T., Meyzen, C., 2004. Pb isotopic analysis of standards and samples using a 207Pb–204Pb double spike and thallium to correct for mass bias with a double-focusing MC-ICP-MS. Chemical Geology 211, 275-303.

Béguelin, P., Chiaradia, M., Beate, B., Spikings, R., 2015. The Yanaurcu volcano (Western Cordillera, Ecuador): A field, petrographic, geochemical, isotopic and geochronological study. Lithos 218-219, 37-53.

Bown, J.W., White, R.S., 1994. Variation with spreading rate of oceanic crustal thickness and geochemistry. Earth and Planetary Science Letters 121, 435-449.

Buiter, S.J.H., Torsvik, T.H., 2014. A review of Wilson Cycle plate margins: A role for mantle plumes in continental break-up along sutures? Gondwana Research 26, 627-653.

Chappell, A.R., Kusznir, N.J., 2008. Three-dimensional gravity inversion for Moho depth at rifted continental margins incorporating a lithosphere thermal gravity anomaly correction. Geophysical Journal International 174, 1-13.

Chen, S.-S., Fan, W.-M., Shi, R.-D., Liu, X.-H., Zhou, X.-J., 2018. 118–115 Ma magmatism in the Tethyan Himalaya igneous province: Constraints on Early Cretaceous rifting of the northern margin of Greater India. Earth and Planetary Science Letters 491, 21-33.

Coffin, M.F., Pringle, M.S., Duncan, R.A., Gladczenko, T.P., Storey, M., Müller, R.D., Gahagan, L.A., 2002. Kerguelen hotspot magma output since 130 Ma. Journal of Petrology 43, 1121-1139.

Coltice, N., Phillips, B.R., Bertrand, H., Ricard, Y., Rey, P., 2007. Global warming of the mantle at the origin of flood basalts over supercontinents. Geology 35, 391-394.

Colwell, J.B., Symonds, P.A., Crawford, A.J., 1994. The nature of the Wallaby (Cuvier) Plateau and other igneous provinces of the west Australian margin. Journal of Australian Geology and Geophysics 15, 137-156.

Condie, K.C., Davaille, A., Aster, R.C., Arndt, N., 2015. Upstairs-downstairs: supercontinents and large igneous provinces, are they related? International Geology Review 57, 1341-1348.

Daczko, N.R., Halpin, J.A., Fitzsimons, I.C.W., Whittaker, J.M., 2018. A cryptic Gondwana-forming orogen located in Antarctica. Scientific Reports 8, 8371.

Direen, N., Cohen, B.E., Maas, R., Frey, F.A., Whittaker, J.M., Coffin, M.F., Meffre, S., Halpin, J.A., Crawford, A.J., 2017. Naturaliste Plateau: constraints on the timing and evolution of the Kerguelen Large Igneous province and its role in Gondwana breakup. Australian Journal of Earth Sciences 64, 851-869.

Doubrovine, P.V., Steinberger, B., Torsvik, T.H., 2012. Absolute plate motions in a reference frame defined by moving hot spots in the Pacific, Atlantic, and Indian oceans. Journal of Geophysical Research: Solid Earth 117, n/a-n/a.

Duncan, R.A., 2002. A Time Frame for Construction of the Kerguelen Plateau and Broken Ridge. Journal of Petrology 43, 1109-1119.

Fitzsimons, I.C.W., 2003. Proterozoic basement provinces of southern and southwestern Australia, and their correlation with Antarctica, in: Yoshida, M., Windley, B.F., Dasgupta, S. (Eds.), Proterozoic East Gondwana: Supercontinent Assembly and Breakup. Geological Society, London, Special Publications, pp. 93-130.

Frey, F.A., McNaughton, N.J., Nelson, D.R., deLaeter, J.R., Duncan, R.A., 1996. Petrogenesis of the Bunbury Basalt, Western Australia: interaction between the Kerguelen plume and Gondwana lithosphere? Earth and Planetary Science Letters 144, 163-183.

Ghatak, A., Basu, A.R., 2011. Vestiges of the Kerguelen plume in the Sylhet Traps, northeastern India. Earth and Planetary Science Letters 308, 52-64.

Gibbons, A.D., Barckhausen, U., van den Bogaard, P., Hoernle, K., Werner, R., Whittaker, J.M., Müller, R.D., 2012. Constraining the Jurassic extent of Greater India: Tectonic evolution of the West Australian margin. Geochemistry, Geophysics, Geosystems 13, Q05W13.

Gibbons, A.D., Whittaker, J.M., Muller, R.D., 2013. The breakup of East Gondwana: Assimilating constraints from Cretaceous ocean basins around India into a best-fit tectonic model. Journal of Geophysical Research-Solid Earth 118, 808-822.

Halpin, J.A., Daczko, N.R., Kobler, M.E., Whittaker, J.M., 2017. Strike-slip tectonics during the Neoproterozoic–Cambrian assembly of East Gondwana: Evidence from a newly discovered microcontinent in the Indian Ocean (Batavia Knoll). Gondwana Research 51, 137-148.

Harris, L.B., 1994. Structural and Tectonic Synthesis for the Perth Basin, Western Australia. Journal of Petroleum Geology 17, 129-156.

Hart, S.R., 1984. A large-scale isotope anomaly in the Southern Hemisphere mantle. Nature 309, 753-757.

Hocking, R.M., 1991. The Silurian Tumblagooda Sandstone, Western Australia. Geological Survey of Western Australia, Report 27.

Ingle, S., Scoates, J.S., Weis, D., Brügmann, G., Kent, R.W., 2004. Origin of Cretaceous continental tholeiites in southwestern Australia and eastern India: insights from Hf and Os isotopes. Chemical Geology 209, 83-106.

Ingle, S., Weis, D., Doucet, S., Mattielli, N., 2003. Hf isotope constraints on mantle sources and shallow-level contaminants during Kerguelen hot spot activity since∼ 120 Ma. Geochemistry, Geophysics, Geosystems 4.

Laske, G., Masters, G., Ma, Z., Pasyanos, M., 2013. Update on CRUST1. 0—A 1-degree global model of Earth's crust, EGU General Assembly, Vienna, Austria, p. 2658.

Lee, J.-Y., Marti, K., Severinghaus, J.P., Kawamura, K., Yoo, H.-S., Lee, J.B., Kim, J.S., 2006. A redetermination of the isotopic abundances of atmospheric Ar. Geochimica et Cosmochimica Acta 70, 4507-4512.

Liu, Z., Zhou, Q., Lai, Y., Qing, C., Li, Y., Wu, J., Xia, X., 2015. Petrogenesis of the Early Cretaceous Laguila bimodal intrusive rocks from the Tethyan Himalaya: Implications for the break-up of Eastern Gondwana. Lithos 236–237, 190-202.

Ma, L., Kerr, A.C., Wang, Q., Jiang, Z.-Q., Hu, W.-L., 2018. Early Cretaceous (~140Ma) aluminous A-type granites in the Tethyan Himalaya, Tibet: Products of crust-mantle interaction during lithospheric extension. Lithos 300-301, 212-226.

Markwitz, V., Kirkland, C.L., Wyrwoll, K.H., Hancock, E.A., Evans, N.J., Lu, Y., 2017. Variations in Zircon Provenance Constrain Age and Geometry of an Early Paleozoic Rift in the Pinjarra Orogen, East Gondwana. Tectonics 36, 2477-2496.

Marzoli, A., Callegaro, S., Dal Corso, J., Davies, J.H.F.L., Chiaradia, M., Youbi, N., Bertrand, H., Reisberg, L., Merle, R., Jourdan, F., 2018. The Central Atlantic Magmatic Province (CAMP): A Review, in: Tanner, L.H. (Ed.), The Late Triassic World: Earth in a Time of Transition. Springer International Publishing, Cham, pp. 91-125.

Matthews, K.J., Seton, M., Müller, R.D., 2012. A global-scale plate reorganization event at 105−100 Ma. Earth and Planetary Science Letters 355–356, 283-298.

McArthur, J.M., Howarth, R.J., Bailey, T.R., 2001. Strontium isotope stratigraphy: LOWESS version 3: best fit to the marine Sr-isotope curve for 0–509 Ma and accompanying look-up table for deriving numerical age. The Journal of Geology 109, 155-170.

Meier, U., Curtis, A., Trampert, J., 2007. Global crustal thickness from neural network inversion of surface wave data. Geophysical Journal International 169, 706-722.

Mole, D.R., Fiorentini, M.L., Thebaud, N., Cassidy, K.F., McCuaig, T.C., Kirkland, C.L., Romano, S.S., Doublier, M.P., Belousova, E.A., Barnes, S.J., 2014. Archean komatiite volcanism controlled by the evolution of early continents. Proceedings of the National Academy of Sciences 111, 10083-10088.

Morant, P., 1988. Donnybrook Project: Annual Report 1988. West Coast Holdings Limited, Perth, <retrieved from http://www.dmp.wa.gov.au/WAMEX-Minerals-Exploration-1476.aspx>.

Murphy, D., Collerson, K., Kamber, B., 2002. Lamproites from Gaussberg, Antarctica: possible transition zone melts of Archaean subducted sediments. Journal of Petrology 43, 981-1001.

Ogg, J.G., 2012. Chapter 5 - Geomagnetic Polarity Time Scale, The Geologic Time Scale. Elsevier, Boston, pp. 85-113.

Olierook, H.K.H., Barham, M., Fitzsimons, I.C.W., Timms, N.E., Jiang, Q., Evans, N.J., McDonald, B.J., 2019. Tectonic controls on sediment provenance evolution in rift basins: Detrital zircon U–Pb and Hf isotope analysis from the Perth Basin, Western Australia. Gondwana Research 66, 126-142.

Olierook, H.K.H., Jourdan, F., Merle, R.E., Timms, N.E., Kusznir, N.J., Muhling, J., 2016. Bunbury Basalt: Gondwana breakup products or earliest vestiges of the Kerguelen mantle plume? Earth and Planetary Science Letters 440, 20-32.

Olierook, H.K.H., Merle, R.E., Jourdan, F., 2017. Toward a Greater Kerguelen large igneous province: Evolving mantle source contributions in and around the Indian Ocean. Lithos 282–283, 163-172.

Olierook, H.K.H., Merle, R.E., Jourdan, F., Sircombe, K., Fraser, G., Timms, N.E., Nelson, G., Dadd, K.A., Kellerson, L., Borissova, I., 2015a. Age and geochemistry of magmatism on the oceanic Wallaby Plateau and implications for the opening of the Indian Ocean. Geology 43, 971-974.

Olierook, H.K.H., Timms, N.E., 2016. Quantifying multiple Permian–Cretaceous exhumation events during the break-up of eastern Gondwana: Sonic transit time analysis of the central and southern Perth Basin. Basin Research 28, 796-826.

Olierook, H.K.H., Timms, N.E., Merle, R.E., Jourdan, F., Wilkes, P.G., 2015b. Paleo-drainage and fault development in the southern Perth Basin, Western Australia during and after the breakup of Gondwana from 3D modelling of the Bunbury Basalt. Australian Journal of Earth Sciences 62, 289-305.

Olierook, H.K.H., Timms, N.E., Wellmann, J.F., Corbel, S., Wilkes, P.G., 2015c. A 3D structural and stratigraphic model of the Perth Basin: Implications for sub-basin evolution. Australian Journal of Earth Sciences 62, 447-467.

Pin, C., Briot, D., Bassin, C., Poitrasson, F., 1994. Concomitant separation of strontium and samarium-neodymium for isotopic analysis in silicate samples, based on specific extraction chromatography. Analytica Chimica Acta 298, 209-217.

Pirajno, F., Santosh, M., 2015. Mantle plumes, supercontinents, intracontinental rifting and mineral systems. Precambrian Research 259, 243-261.

Playford, P.E., Cockbain, A.E., Low, G.H., 1976. Geology of the Perth Basin, Western Australia. Geological Survey of Western Australia, Perth, pp. 1-323, <retrieved from http://geodocs.dmp.wa.gov.au/>.

Poynton, D.J., Hollams, R.F.F., 1980. Whicher Range No. 2 well completion report. Mesa Australia Limited, Perth, <retrieved from http://www.dmp.wa.gov.au/4187.aspx>.

Renne, P.R., Balco, G., Ludwig, K.R., Mundil, R., Min, K., 2011. Response to the comment by W.H. Schwarz et al. on "Joint determination of ^{40}K decay constants and ^{40}Ar*/^{40}K for the Fish Canyon sanidine standard, and improved accuracy for $^{40}Ar/^{39}Ar$ geochronology" by PR Renne et al. (2010). Geochimica et Cosmochimica Acta 75, 5097-5100.

Shi, Y., Hou, C., Anderson, J.L., Yang, T., Ma, Y., Bian, W., Jin, J., 2018. Zircon SHRIMP U–Pb age of Late Jurassic OIB-type volcanic rocks from the Tethyan Himalaya: constraints on the initial activity time of the Kerguelen mantle plume. Acta Geochimica 37, 441-455.

Song, T., Cawood, P.A., 2000. Structural styles in the Perth Basin associated with the Mesozoic break-up of Greater India and Australia. Tectonophysics 317, 55-72.

Spencer, C.J., Kirkland, C.L., Taylor, R.J.M., 2016. Strategies towards statistically robust interpretations of in situ U–Pb zircon geochronology. Geoscience Frontiers 7, 581-589.

Storey, M., Kent, R., Saunders, A., Salters, V., Hergt, J., Whitechurch, H., Sevigny, J., Thirlwall, M., Leat, P., Ghose, N., 1992. Lower Cretaceous volcanic rocks on continental margins and their relationship to the Kerguelen Plateau, Proceedings of the Ocean Drilling Program, scientific results, pp. 33-53.

Sushchevskaya, N.M., Migdisova, N.A., Antonov, A.V., Krymsky, R.S., Belyatsky, B.V., Kuzmin, D.V., Bychkova, Y.V., 2014. Geochemical features of the quaternary lamproitic lavas of Gaussberg Volcano, East Antarctica: Result of the impact of the Kerguelen plume. Geochemistry International 52, 1030-1048.

Tanaka, T., Togashi, S., Kamioka, H., Amakawa, H., Kagami, H., Hamamoto, T., Yuhara, M., Orihashi, Y., Yoneda, S., Shimizu, H., Kunimaru, T., Takahashi, K., Yanagi, T., Nakano, T., Fujimaki, H., Shinjo, R., Asahara, Y., Tanimizu, M., Dragusanu, C., 2000. JNdi-1: a neodymium isotopic reference in consistency with LaJolla neodymium. Chemical Geology 168, 279-281.

Union Oil Development Corporation, 1972. Wonnerup No. 1 well, Western Australia, well completion report, Toowoomba, Queensland, <retrieved from http://www.dmp.wa.gov.au/4187.aspx>.

Veevers, J.J., 2004. Gondwanaland from 650–500 Ma assembly through 320 Ma merger in Pangea to 185–100 Ma breakup: supercontinental tectonics via stratigraphy and radiometric dating. Earth-Science Reviews 68, 1-132.

Verati, C., Jourdan, F., 2014. Modelling effect of sericitization of plagioclase on the $^{40}K/^{40}Ar$ and $^{40}K/^{39}Ar$ chronometers: Implication for dating basaltic rocks and mineral deposits. Geological Society Special Publication 378, 155-174.

Ware, B., Jourdan, F., 2018. 40Ar/39Ar geochronology of terrestrial pyroxene. Geochimica et Cosmochimica Acta 230, 112-136.

Watson, S.J., Whittaker, J.M., Halpin, J.A., Williams, S.E., Milan, L.A., Daczko, N.R., Wyman, D.A., 2016. Tectonic drivers and the influence of the Kerguelen plume on seafloor spreading during formation of the early Indian Ocean. Gondwana Research 35, 97-114.

Weis, D., Frey, F., Leyrit, H., Gautier, I., 1993. Kerguelen Archipelago revisited: geochemical and isotopic study of the Southeast Province lavas. Earth and Planetary Science Letters 118, 101-119.

Wharton, P.H., 1981. The geology and hydrogeology of the Quindalup borehole line, Annual Report for 1980. Western Australia Geological Survey, Perth, <retrieved from http://geodocs.dmp.wa.gov.au/>, pp. 27-35.

White, R.S., McKenzie, D., O'Nions, R.K., 1992. Oceanic crustal thickness from seismic measurements and rare earth element inversions. Journal of Geophysical Research: Solid Earth 97, 19683-19715.

Whittaker, J.M., Williams, S.E., Halpin, J.A., Wild, T.J., Stilwell, J.D., Jourdan, F., Daczko, N.R., 2016. Eastern Indian Ocean microcontinent formation driven by plate motion changes. Earth and Planetary Science Letters 454, 203-212.

Whittaker, J.M., Williams, S.E., Müller, R.D., 2013. Revised tectonic evolution of the Eastern Indian Ocean. Geochemistry, Geophysics, Geosystems 14, 1891-1909.

Will, T.M., Frimmel, H.E., 2018. Where does a continent prefer to break up? Some lessons from the South Atlantic margins. Gondwana Research 53, 9-19.

Williams, C.T., Nicholls, J., 1966. Sue 1 well completion report, S-series (S268) Open file Report, Microfilm Roll 43. Western Australia Geological Survey, Perth, <retrieved from http://www.dmp.wa.gov.au/4187.aspx>.

Young, A., Flament, N., Maloney, K., Williams, S., Matthews, K., Zahirovic, S., Müller, R.D., 2018. Global kinematics of tectonic plates and subduction zones since the late Paleozoic Era. Geoscience Frontiers.

Zhu, D.-C., Chung, S.-L., Mo, X.-X., Zhao, Z.-D., Niu, Y., Song, B., Yang, Y.-H., 2009. The 132 Ma Comei-Bunbury large igneous province: Remnants identified in present-day southeastern Tibet and southwestern Australia. Geology 37, 583-586.

Figure captions

Fig. 1: (a) Bathymetric map of the Indian Ocean in the vicinity of the margin of Western Australia, after Amante & Eakins (2009). Major bathymetric features of the Indian Ocean, and locations and ages of dated extrusive rocks recovered from DSDP, ODP, IODP and industry volcanic basement sites are indicated after Olierook et al. (2017). (b) Map of onshore southwestern Australia showing the

position and ages of the Bunbury Basalt, modified from Olierook et al. (2015b) with age data from Olierook et al. (2016) and this study.

Fig. 2: $^{40}Ar/^{39}Ar$ apparent age and related K/Ca ratio spectra of the plagioclase separates versus the cumulative percentage of ^{39}Ar released. Errors on plateau ages are quoted at 2σ. See Supplementary Table A for full data.

Fig. 3: Weighted mean of individual $^{40}Ar/^{39}Ar$ plateau steps from the Donnybrook Paleovalley.

Fig. 4: Sr–Nd–Pb isotopic data for the Bunbury Basalt, including previously published data from Storey et al. (1992), Colwell et al. (1994) and Frey et al. (1996). Assigned ages are from Coffin et al. (2002), Olierook et al. (2016) and this study. Where samples have not been dated (i.e., age uncertainty), extrapolation of lava flows using a 3D model of the Bunbury Basalt was employed (Olierook et al., 2015b). Analytical uncertainties are smaller than the symbol sizes. NHRL = Northern Hemisphere Reference Line (Hart, 1984). Axes dimensions are equivalent to the entire Greater Kerguelen LIP dataset in Fig. 7.

Fig. 5: Age progression of Greater Kerguelen LIP magmatism with longitude. (a) Southwestern Australia, showing the evolution of basin-wide magmatism at ca. 137–136 Ma, to restriction at ca. 133 Ma and localization at ca. 130.5 Ma (Coffin et al., 2002; Olierook et al., 2016; this study). (b) Southwestern Australia and Naturaliste Plateau, showing further younging of magmatism offshore (Direen et al., 2017; Olierook et al., 2017).

Fig. 6: Age data comparison from pre-95 Ma volcanism attributed to the Greater Kerguelen large igneous province, the timing of continental breakup, magnetic anomalies and stratigraphic data constraints, modified from Whittaker et al. (2016), and recalculated and filtered for reliable data. Our criteria for reliability are: (a) all data have $p > 0.05$, (b) $^{40}Ar/^{39}Ar$ plateau ages have >70% ^{39}Ar and at least three consecutive steps, (c) U–Pb analyses are concordant (Spencer et al., 2016), (d) all uncertainties are less than 5 Ma at 2σ (~4–5%). See Supplementary Table C for data compilation and references.

Fig. 7: Compilation of Sr–Nd–Pb isotopic data from the Greater Kerguelen large igneous province, modified from Olierook et al. (2017). Mantle sources: asthenospheric depleted mantle source from Southeast Indian Ridge (cf. Olierook et al., 2017), Kerguelen mantle plume from Kerguelen Archipelago (Weis et al., 1993), Greater Indian continental crust from northeastern India (Ghatak and Basu, 2011) and lithospheric source from ultrapotassic rocks in Antarctica (Sushchevskaya et al., 2014). For detailed rationale for mantle sources, see section 4.4 in Olierook et al. (2017). In this study, analyses were filtered for loss-on-ignition (LOI < 2%). Where LOI was not reported, symbols are semi-transparent. For a full list of sources, see Supplementary Table D. Analytical uncertainties are smaller than the symbol sizes. NHRL = Northern Hemisphere Reference Line (Hart, 1984).

Fig. 8: Plate and plume reconstructions and schematic cross-sections showing the breakup of eastern Gondwana, the arrival and impingement of the Kerguelen mantle plume, and magmatic production in eastern Gondwana at key time periods, modified from Olierook et al. (2017). (a) 147 Ma: earliest magmatic products in eastern Gondwana in the Tethyan Himalaya (Shi et al., 2018). (b) 137 Ma:

rupture of the continental lithosphere and onset of the Bunbury Basalt (Gibbons et al., 2013; Olierook et al., 2016). (c) 130 Ma: end of magmatism in onshore southwestern Australia (Olierook et al., 2016). (d) 124 Ma: magmatism on Wallaby Plateau immediately prior to onset of magmatism on the Kerguelen Plateau (Olierook et al., 2015a). (e) 100 Ma: towards end of global plate reorganization (Matthews et al., 2012) and . AR = Argoland, B = Batavia Knoll, BB = Bunbury Basalt, CKP = Central Kerguelen Plateau, EB = Elan Bank, EP = Exmouth Plateau, G = Gulden Draak Knoll, GB = Gascoyne Block, N = Naturaliste Plateau, PCM = Prince Charles Mountains, R = Rajmahal–Bengal–Sylhet Traps, SKP = Southern Kerguelen Plateau, TH = Tethyan Himalaya, W = Wallaby Plateau, Z = Zenith Plateau.

Table 1: Location of newly-collected samples for the Bunbury Basalt lava flows. Flow context from Olierook et al. (2015b). Pv. = Paleovalley.

Table 2: Summary of plateau and inverse isochrons ages for concordant $^{40}Ar/^{39}Ar$ lava flow analyses.

Supplementary Table A: Full $^{40}Ar/^{39}Ar$ data for new analyses from the Donnybrook Paleovalley.

Supplementary Table B: New major and trace element data, and Sr–Nd–Pb isotopic data. Previously published major and trace element data for BN3, BN4, BN10, BN21 and BN22 from Olierook et al. (2016).

Supplementary Table C: Compilation of statistically-reliable geochronological data from the Greater Kerguelen Plateau.

Supplementary Table D: Compilation of Sr–Nd–Pb isotopic analyses from the Greater Kerguelen large igneous province.

Figure 1

Click here to download Figure: Figure 1_Indian Ocean + SPB map.pdf

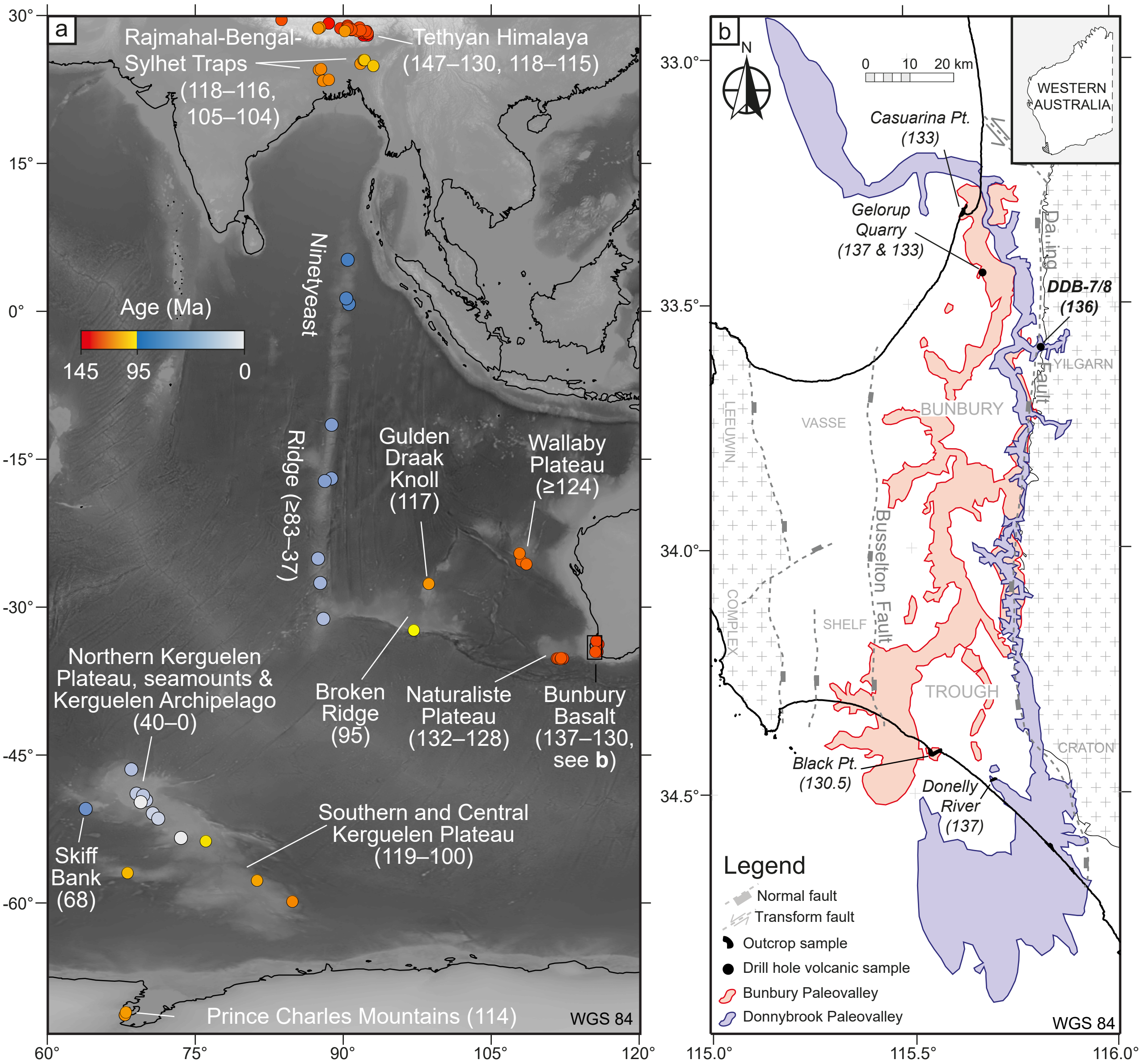

Olierook et al., Figure 1

Figure 2

Click here to download Figure: Figure 2_Ar-Ar ARGUS.pdf

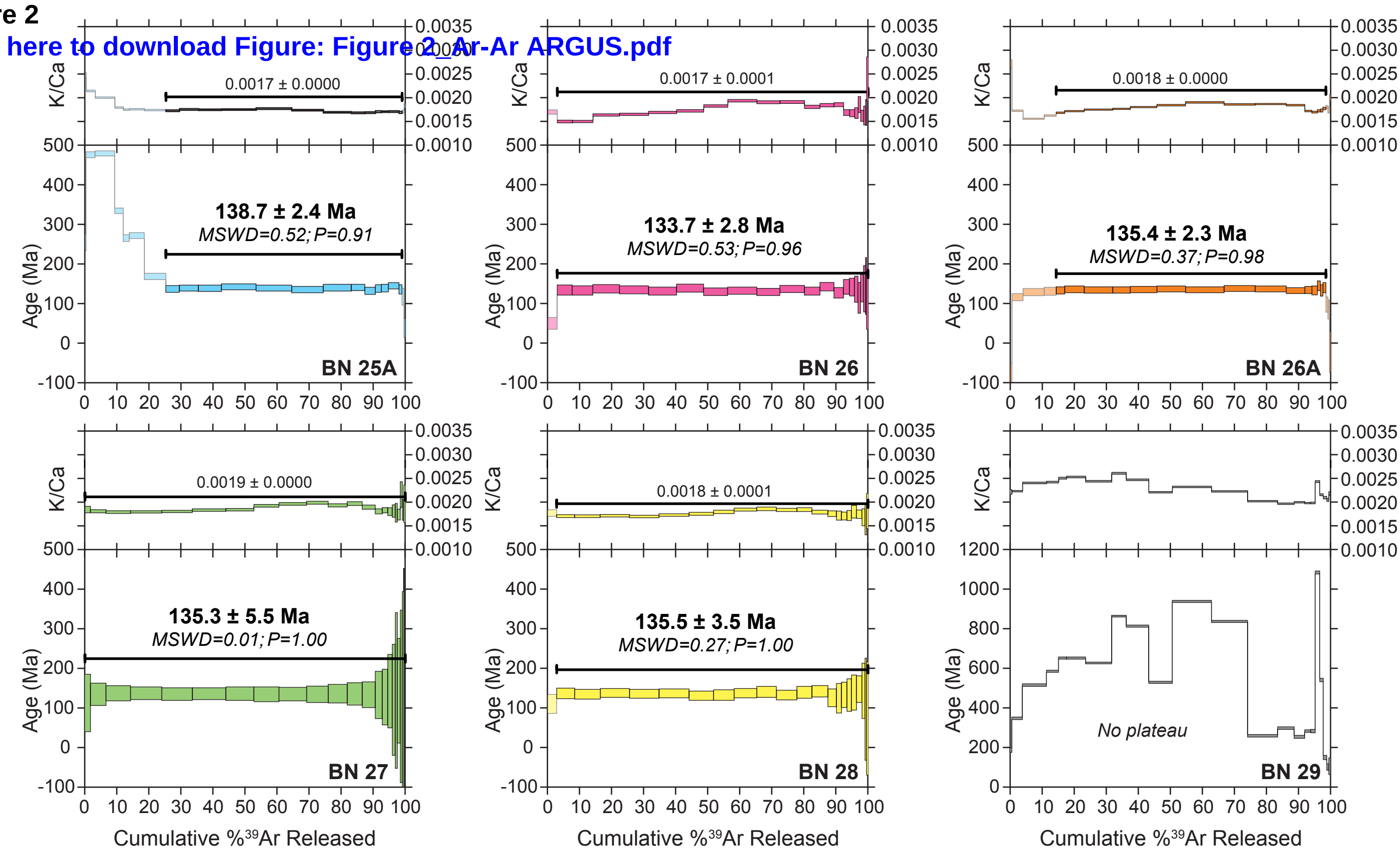

Olierook et al., Figure 2

Figure 3

Click here to download Figure: Figure 3 Age plot.pdf

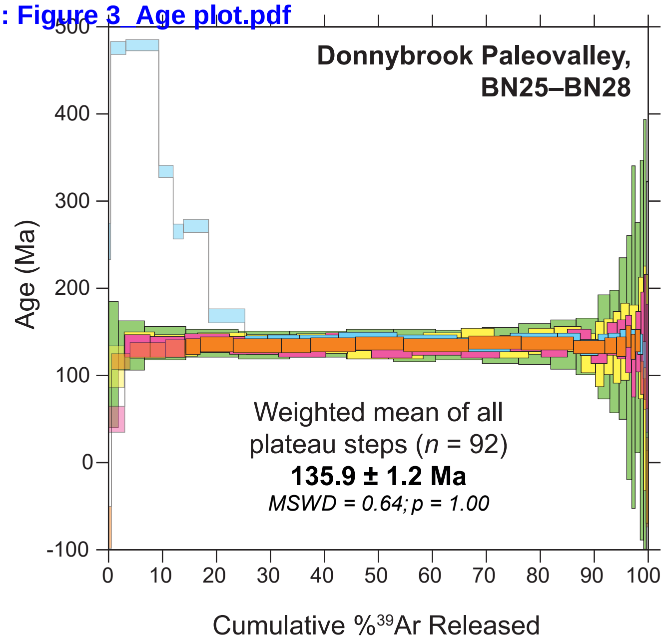

Olierook et al., Figure 3

Figure 4

Click here to download Figure: Figure 4_Geochemistry isotopes Bunbury.pdf

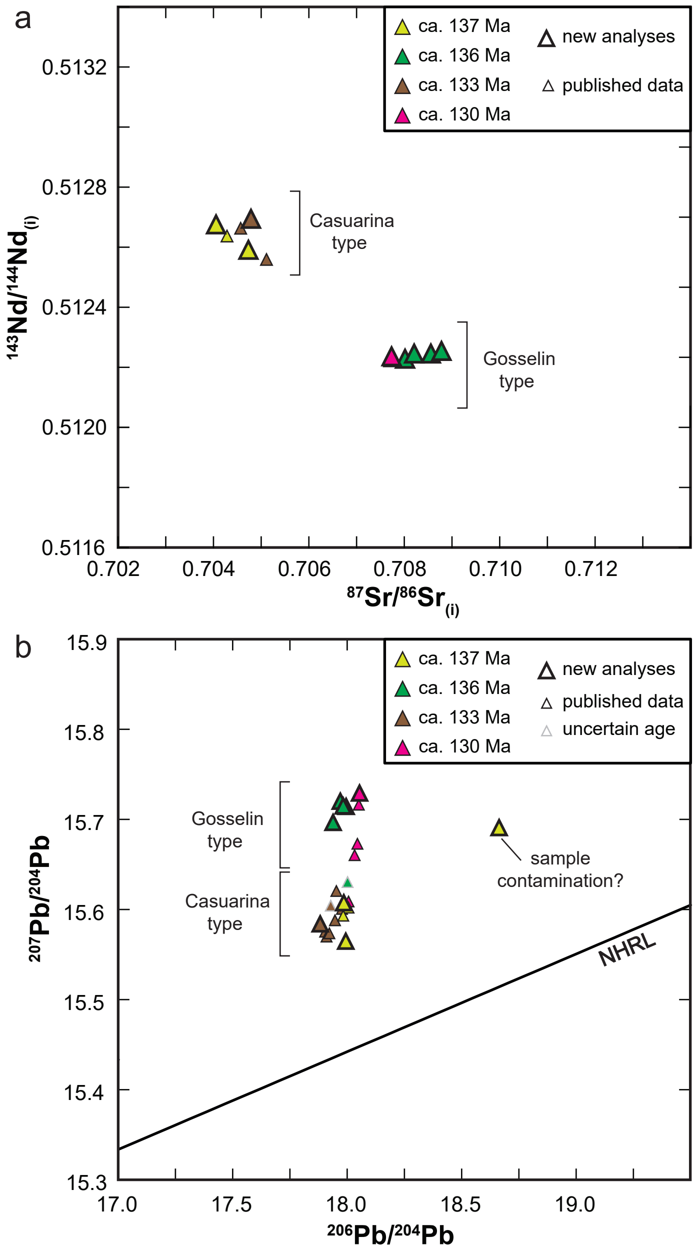

Olierook et al., Figure 4

Figure 5

Click here to download Figure: Figure 5_Age vs longitude.pdf

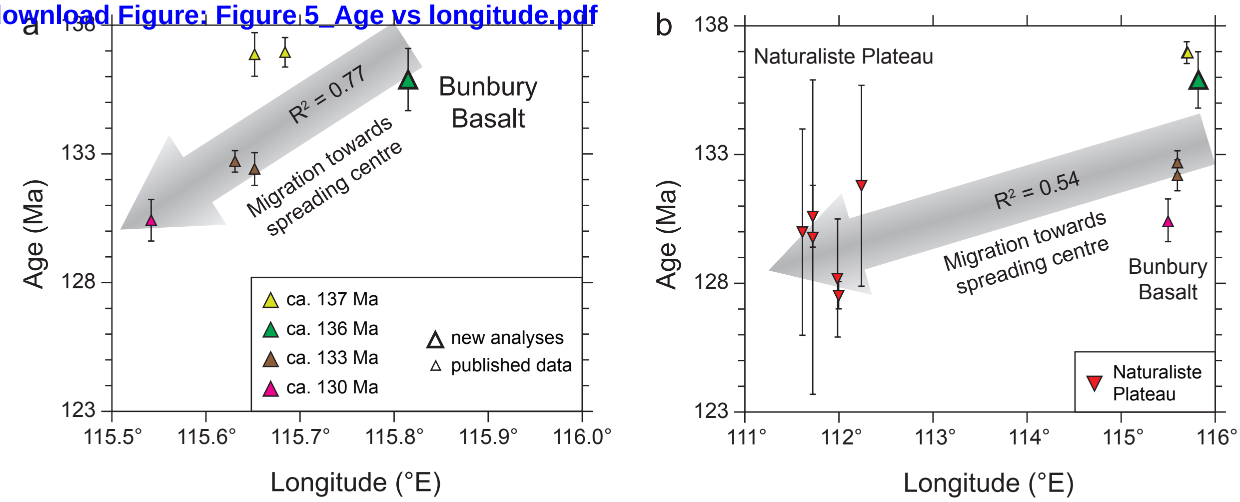

Olierook et al., Figure 5

Figure 6

Click here to download Figure: Figure 6_Age comparison.pdf

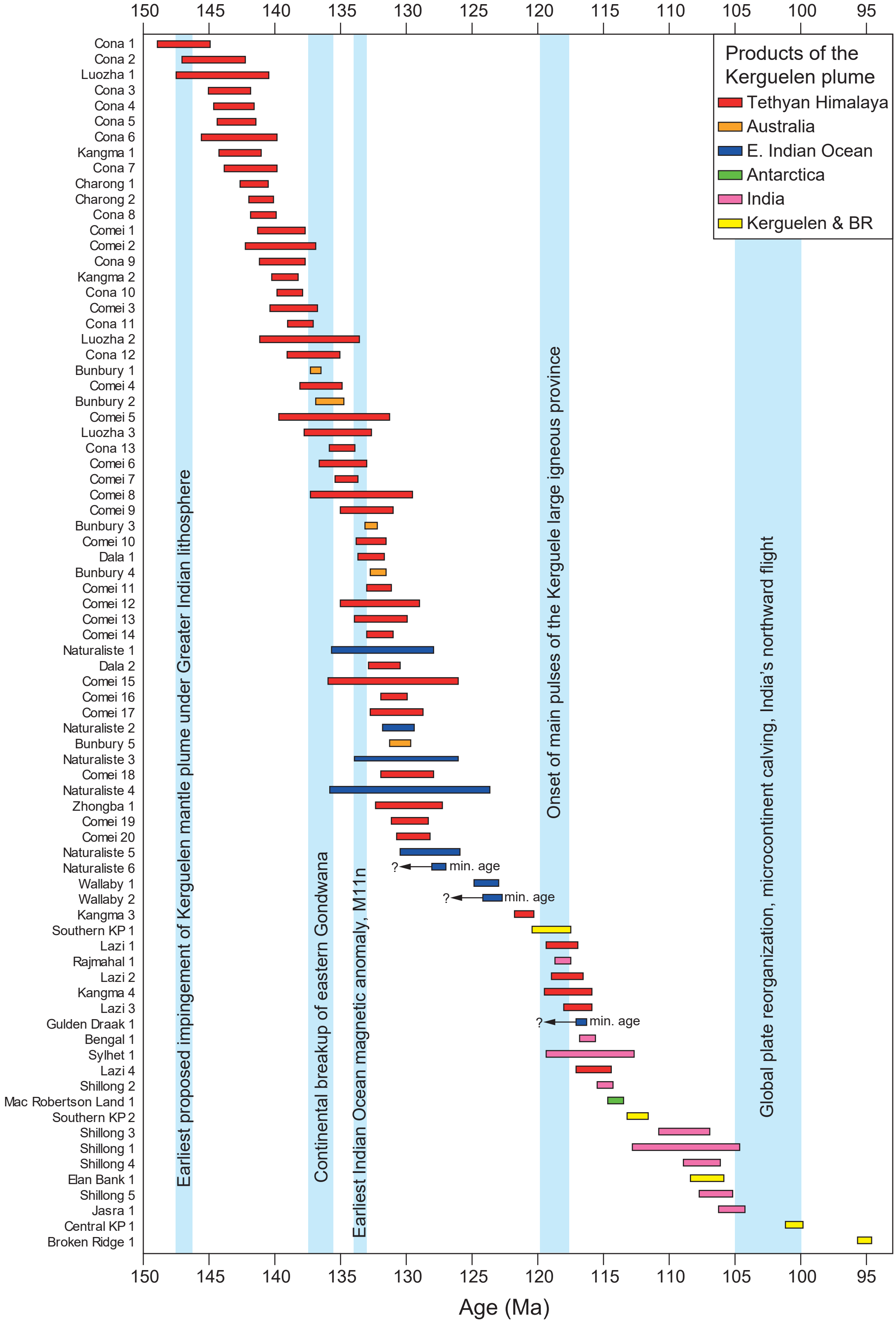

Olierook et al., Figure 6

Figure 7

Click here to download Figure: Figure 7_Geochemistry isotopes _v2.pdf

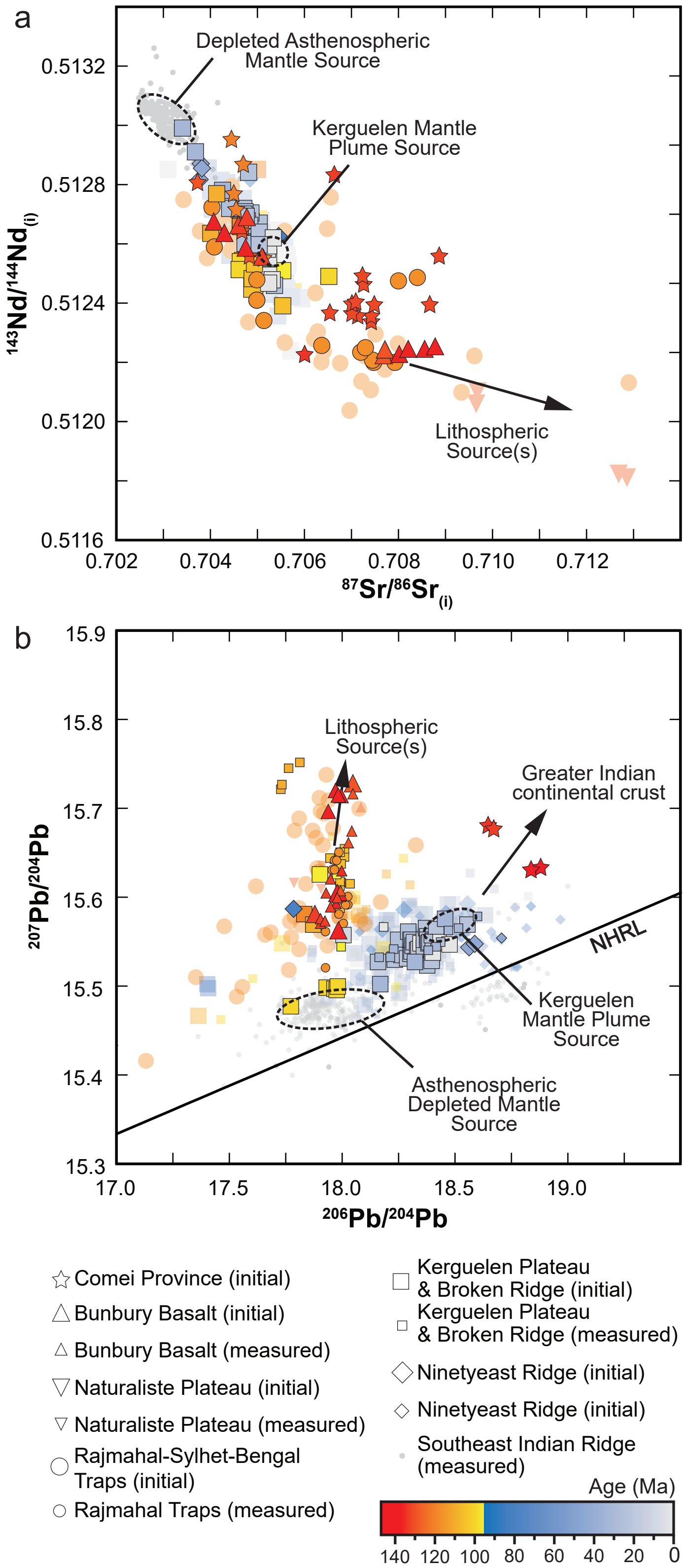

Olierook et al., Figure 7

Figure 8

Click here to download Figure: Figure 8_Gplates reconstruction_v2.pdf

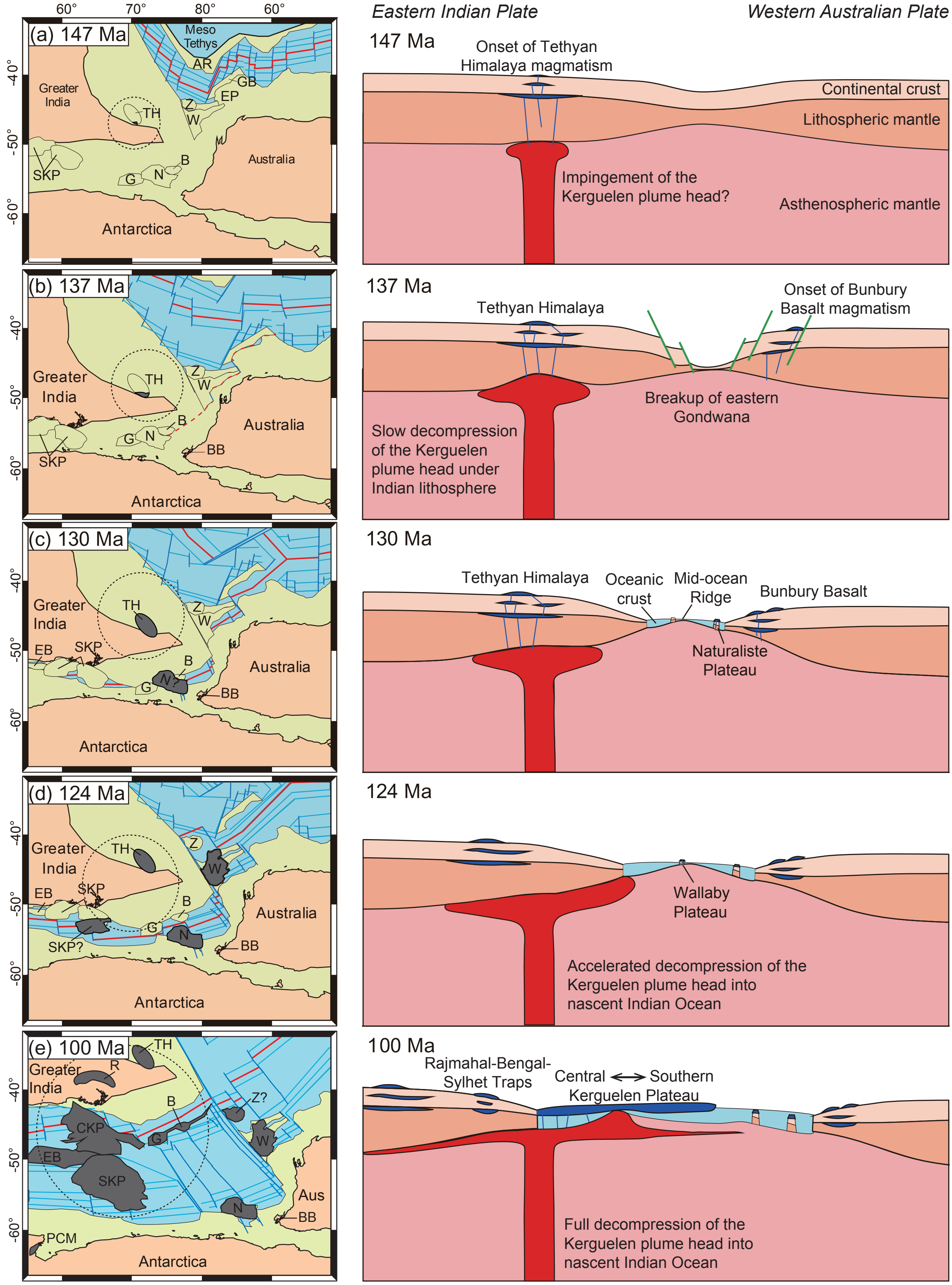

Olierook et al., Figure 8

Table 1

Click here to download Table: Table 1_Donnybrook Paleovalley sample list.xlsx

Sample no.	Coordinates[a]		Well/Area name	Flow context	Depth (m)	
	Latitude	Longitude			Start	End
BN25	–33.59299	115.81622	Donnybrook 7, DDB7	Donnybrook Paleovalley	173.1	173.3
BN26	–33.59299	115.81622	Donnybrook 7, DDB7	Donnybrook Paleovalley	191.1	191.3
BN27	–33.59299	115.81622	Donnybrook 7, DDB7	Donnybrook Paleovalley	218.5	218.7
BN28	–33.77329	115.81208	Donnybrook 8, DDB8	Donnybrook Paleovalley	177.5	177.7
BN29	–33.77329	115.81208	Donnybrook 8, DDB8	Donnybrook Paleovalley	203.5	203.7

[a]All coordinates used GCS WGS84, and were determined by GPS (± 5m)

Olierook et al., Table 1

Table 2
Click here to download Table: Table 2_ARGUS Ar-Ar results_v1.xlsx

General characteristics		Plateau characteristics				Isochron characteristics					
Sample no	**K/Ca**	**Plateau Age (Ma ± 2σ)**	**Total ^{39}Ar Released (%)**	**MSWD**	***p***	**Inv. Isochron Age (Ma ± 2σ)**	**n**	**$^{40}Ar/^{36}Ar$ Intercept (± 2σ)**	**MSWD**	***p***	**Spreading factor (%)**
BN 25A	0.0017	138.7 ± 2.4	74	0.52	0.91	139 ± 4	13	298 ± 5	0.55	0.87	43
BN 26	0.0017	133.7 ± 2.8	97	0.53	0.96	135 ± 5	21	296 ± 10	0.54	0.94	58
BN 26A	0.0018	135.4 ± 2.3	84	0.37	0.98	135 ± 4	15	299 ± 6	0.4	0.98	45
BN 27	0.0019	135.3 ± 5.5	100	0.03	1.00	137 ± 10	22	293 ± 35	0.03	1.00	67
BN 28	0.0018	135.5 ± 3.5	97	0.29	1.00	138 ± 6	21	289 ± 21	0.27	1.00	62
BN 29A	0.0022	*No plateau age*									
ighted mean of plateau steps:		**135.9 ± 1.2**	***n* = 92**	**0.63**	**1.00**						

[a]MSWD and probability of fit (p) for plateau and isochron, percentage of ^{39}Ar degassed used in the plateau calculation, number of analyses included in the isochron, and $^{40}Ar/^{36}Ar$ intercept are indicated. Analytical uncertainties on the ages are quoted at 2 sigma (2σ) confidence levels.

Olierook et al., Table 2

Supplementary Table A

Click here to download Supplementary material for online publication only: Supplementary Table A_Full Ar-Ar data.xlsx

Supplementary Table B
Click here to download Supplementary material for online publication only: Supplementary Table B_Geochemistry.xlsx

Supplementary Table C

Click here to download Supplementary material for online publication only: Supplementary Table C_ Age compilation_v2.xlsx

Supplementary Table D
Click here to download Supplementary material for online publication only: Supplementary Table D_Geochem compilation_v2.xl